Supplementary Information

In-situ organic cation evolution driven sequential crystal transformation in hybrid metal halides

Wenqing Han, Junjie Guan, Xufan Guo, Wenting Liu, Ruijia Zhao, Zhihua Wang, Lin Xu, Puxin Cheng, Minghui Chen, Quanwen Li, Danhong Wang, Jialiang Xu*, and Xian-He Bu

School of Materials Science and Engineering, Tianjin Key Laboratory of Metal and Molecular Materials Chemistry, Frontiers Science Center for New Organic Matter, Academy for Advanced Interdisciplinary Studies, Nankai University, Tianjin 300350, P. R. China

*Correspondence to: jialiang.xu@nankai.edu.cn (J. Xu)

Table of Contents

Materials

Chemicals, such as bismuth bromide ($BiBr_3$, Maclin, 98%), antimony tribromide ($SbBr_3$, Maclin, 99.99%), hydrobromic acid (HBr, Maclin, 40 wt%. in water), dimethyl sulfoxide (DMSO, Maclin, 99.8%), acetone (Gaofeng, 99.7%), were commercially purchased and used without further purification.

Synthesis of OIHMHs

Liquid-phase diffusion crystallization system

$BiBr_3$ (89.7 mg, 0.2 mmol) or $SbBr_3$ (72.3 mg, 0.2 mmol) was dissolved in a mixture of DMSO (1.0 mL) and HBr (0.5 mL, 40 wt%) in a vial. The mixture was ultrasonically processed at room temperature until it became clear. Then, 4.0 mL of acetone was slowly added to the vial along the inside. Transparent bulk $(DOPS)_4[Bi/SbBr_6]Br$, $(DOPS)_2(TMS)[Bi/SbBr_6]$, and $(TMS)_4$-$[Bi/SbBr_6]Br$ mixed crystals could be obtained through liquid-phase diffusion crystallization after 3 days at 20 °C. All crystal samples were separated from the mother liquor by pressure reduction and filtration, washed with ethanol, and dried in a vacuum oven at 25 °C for one day.

Vapor-phase evaporation crystallization system

$BiBr_3$ (89.7 mg, 0.2 mmol) or $SbBr_3$ (72.3 mg, 0.2 mmol) was dissolved in a mixture of DMSO (1.0 mL) and HBr (0.5 mL, 40 wt%) in a vial. The mixture was ultrasonically processed at room temperature until it became clear. The vial with the precursor solution was placed into a larger glass bottle containing 20.0 mL of acetone as the antisolvent. Transparent bulk crystals of $(DOPS)_4[Bi/SbBr_6]Br$ could be obtained through antisolvent vaporization crystallization after 3 days at 12~20 °C. $(DOPS)_2(TMS)[Bi/SbBr_6]$ could be obtained after 3 days at 25~35 °C. $(TMS)_4[Bi/SbBr_6]Br$ could be obtained after 3 days at 50~65 °C. All crystal samples were separated from the mother liquor by pressure reduction and filtration, washed with ethanol, and dried in a vacuum oven at 25 °C for one day.

Structural analyses and characterizations

^{1}H NMR spectra were obtained on a Varian Mercury Vx 300 spectrometer at 400 MHz, with DMSO-d_6 as the solvent. ^{13}C NMR spectra were obtained on a Varian Mercury Vx 300 spectrometer at 100 MHz, with DMSO-d_6 as the solvent. Mass spectra (MS) were measured by VG ZAB-HS chromatography-mass spectrometry. The multi-scan mode collected SCXRD data was collected on a Rigaku XtalAB PRO MM007 DW diffractometer under Cu Kα radiation (λ = 1.5418 Å). The SHELXT methods with the Olex2 program51 were employed to determine the single crystal structures. The anisotropic refinement of all non-hydrogen atoms was performed by the SHELXL method and the least-squares technique. When the structure shows split electron density peaks for certain atoms (especially light atoms like O, S or C), a disorder model is appropriate. PART command was used correctly to handle disorder in the cifs of $(DOPS)_2(TMS)[Bi/SbBr_6]$. DFIX was used to constrain specific bond lengths when disorder causes unrealistic bond length deviations. OMIT was only employed for reflections that showed clear measurement errors or were outside the expected range. PXRD measurements were performed using a Rigaku MiniFlex600 diffractometer at 40 kV, 100 mA, with a Cu-target tube and a graphite monochromator. TGA experiments were carried out using a thermal analyzer (TA Instruments Q50) under an Ar atmosphere in the temperature range of 30 to 800 °C, with a heating rate of 10 °C min^{-1}. UV-vis transmission spectra were measured on the solid powder sample using a UV-vis spectrophotometer (UV 2600). The data from "absorption" to the tauc plot according to the $(\alpha hv)^{1/n} = A(hv - Eg)$ with the direct bandgap select n = 1/2.[1] FTIR spectra were collected on a TENSOR II spectrometer from 4000 to 400 cm^{-1}. PL measurements (including PL spectra, lifetime spectra, time-resolved emission spectra and quantum yield data) were carried out using an Edinburgh FS5 fluorescence spectrometer. Lifetime spectra were collected under the 100 Hz microsecond lamp source and the instrument response function (IRF) curve was recorded from the decay signals of the excitation sources.

NLO measurements

TPF measurements were carried out with a home-built multiphoton NLO microscope system.[2, 3] A commercial femtosecond pump laser (Mai Tai HP, wavelength ranging from 690 to 1040 nm, pulse width: ~100 fs, frequency: 80 MHz) was used in the reflection geometry, with both the incidence and detection angles set at 45 degree. The TPF signal reflected from the front surface of

the crystals was detected. Power-dependent TPF spectra were obtained by increasing the laser power at 800 nm laser excitation until the signals were saturated. The laser spot was ~20 μm in diameter.

Supplementary Figures

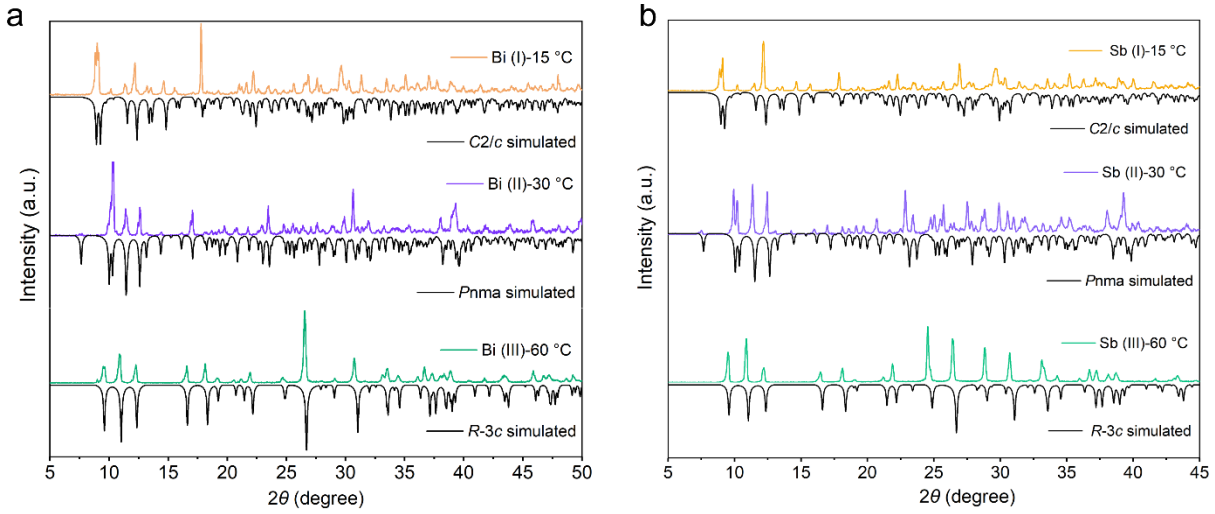

Figure S1 PXRD patterns of three types of OIHMH (Bi-/Sb-based) samples compared with calculated PXRD patterns, showing a considerable phase purity of the resulting OIHMHs containing the *in-situ* synthesized organic cations under ambient conditions.

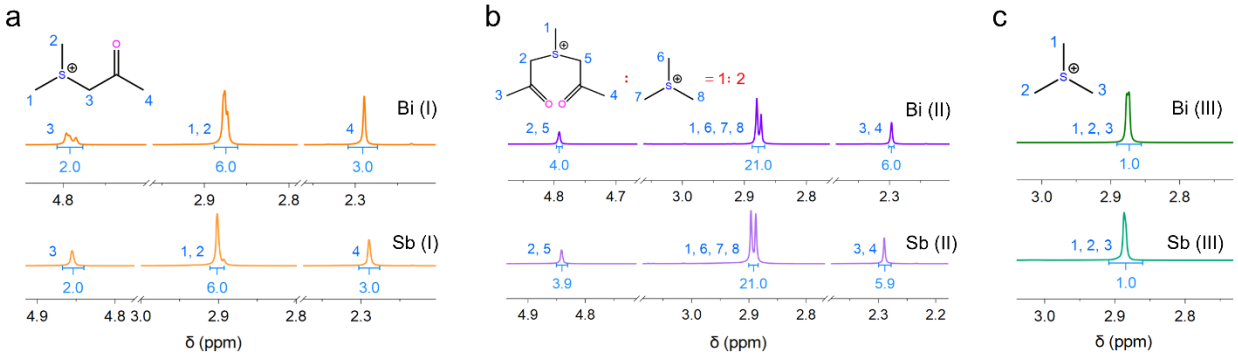

Figure S2 ^{1}H NMR spectra of the dissolved Bi- and Sb-based crystals, confirming that the *in-situ* synthesized $DOPS^{+}$ and TMS^{+} are involved in the dissolved sample from the as-formed OIHMH crystals.

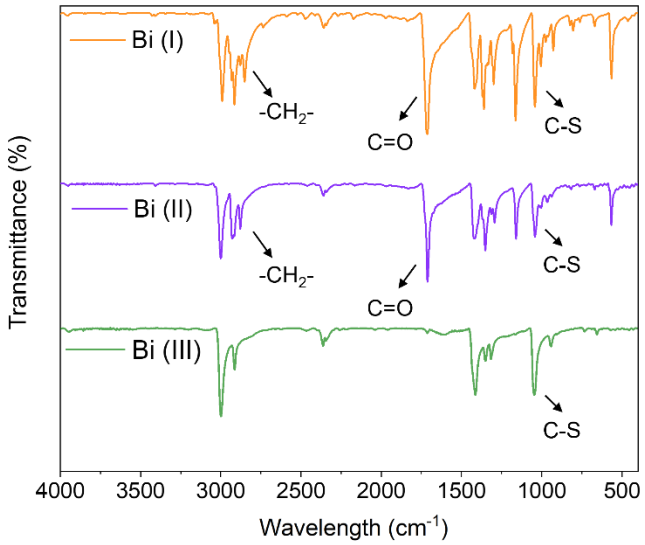

Figure S3 FTIR spectra of the three Bi-based OIHMHs. Characteristic peaks of the C=O group (at 1711 cm^{-1}) and the -CH_2- group (at 2850 cm^{-1}) are present in Bi (I) and Bi (II) but absent in Bi (III), verifying the different organic components in these three OIHMHs.

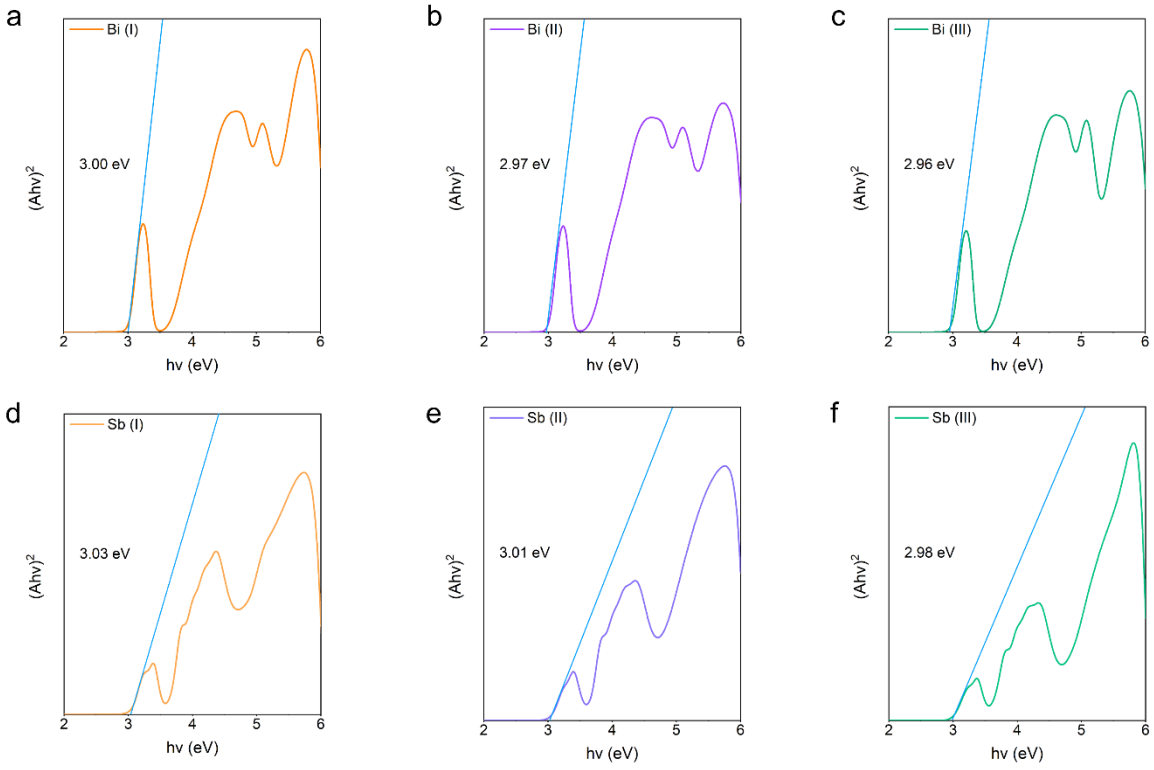

Figure S4 Calculated optical bandgaps (E_g) from the UV-vis absorption edge of the three types of OIHMHs.

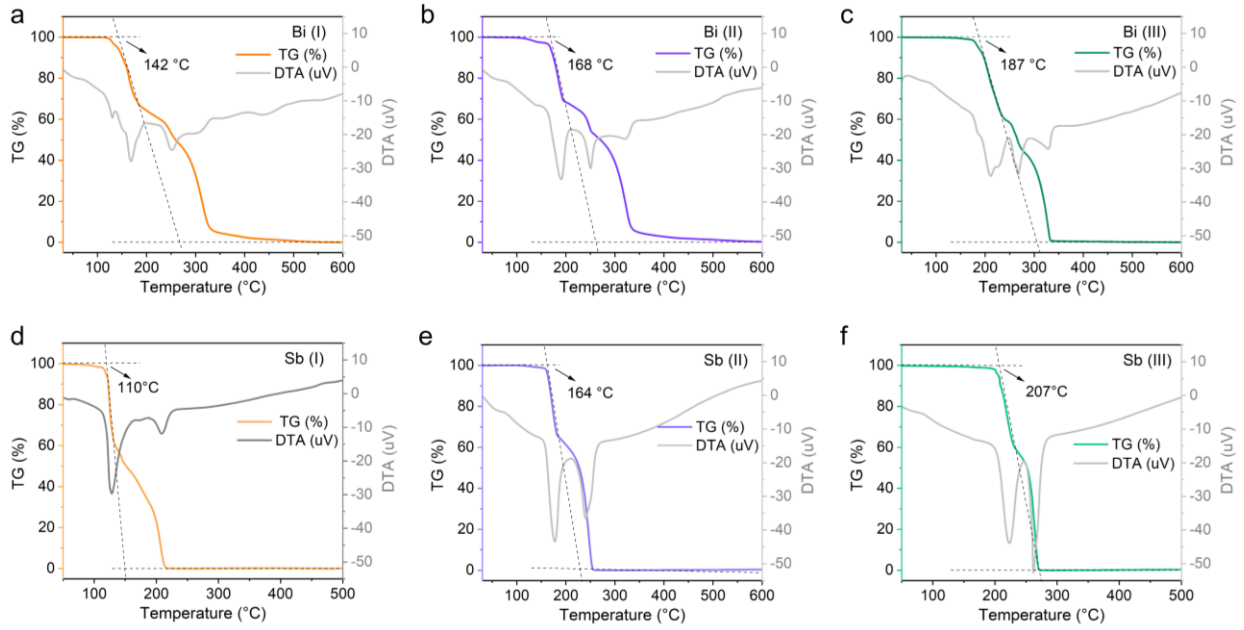

Figure S5 TGA curves of the three types of OIHMHs.

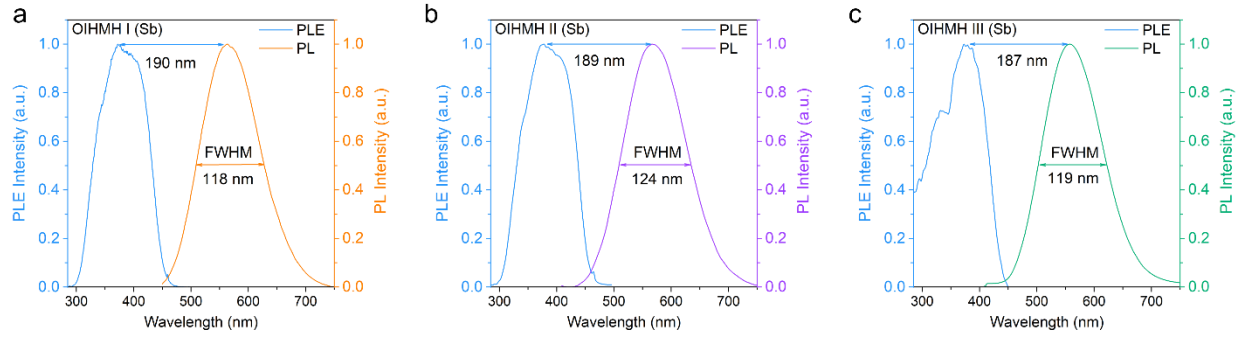

Figure S6 Normalized PL, PLE spectra of the three Sb-based OIHMHs.

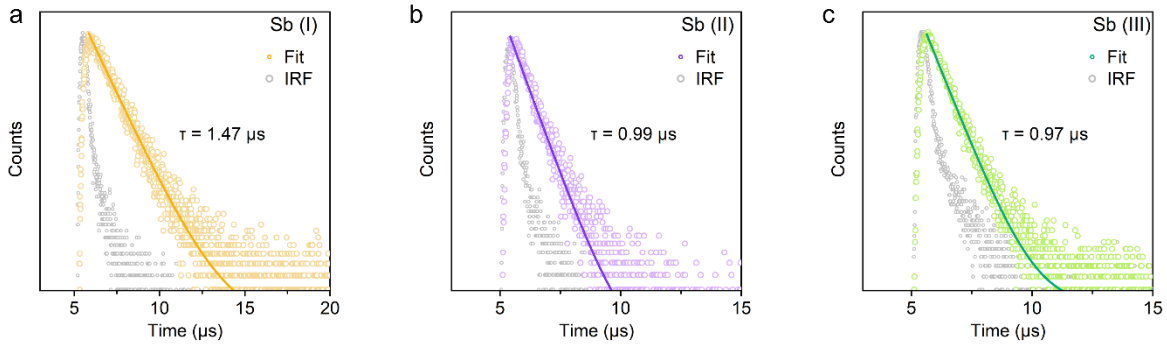

Figure S7 PL decay spectra of the three Sb-based OIHMHs. All time-resolved decay PL spectra could be well fitted to a mono-exponential function with τ = 1.47 μs, 0.99 μs, and 0.97 μs, respectively, signifying the triple STE ($^3P_1$ / $^1S_0$) electronic transition process.

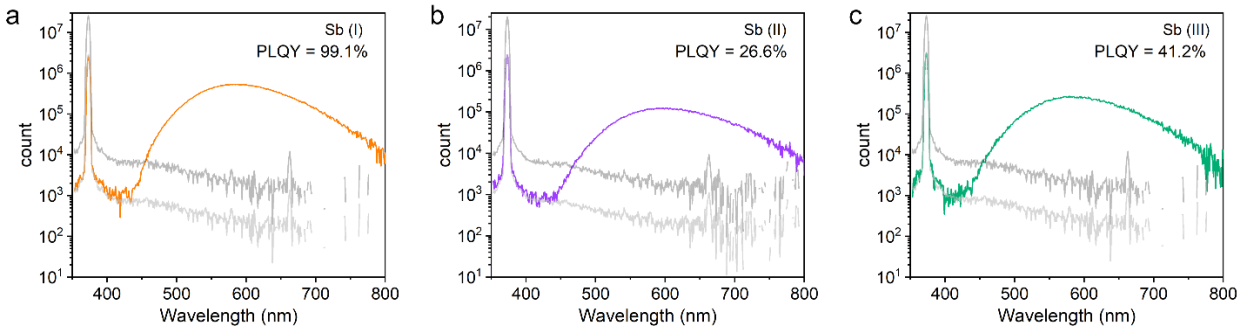

Figure S8 PLQY spectra of the three Sb-based OIHMH crystals excited by their optimal excitation wavelength UV light.

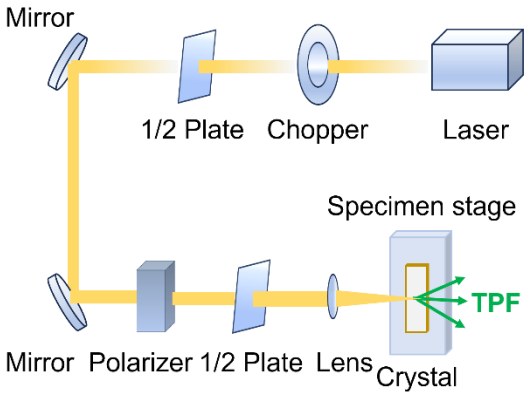

Figure S9 The diagram of the TPF testing device.

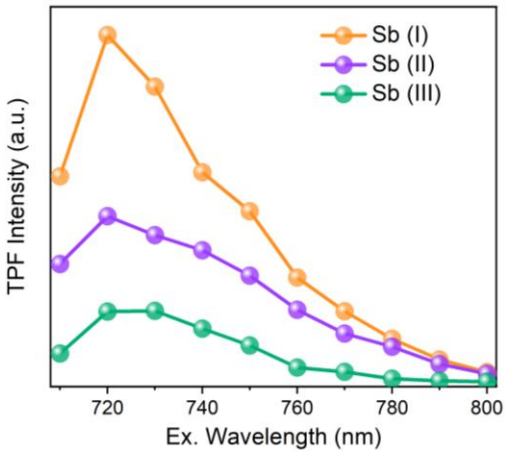

Figure S10 TPF spectra of three Sb-based OIHMH crystals under excitation with a range from 720 nm to 800 nm.

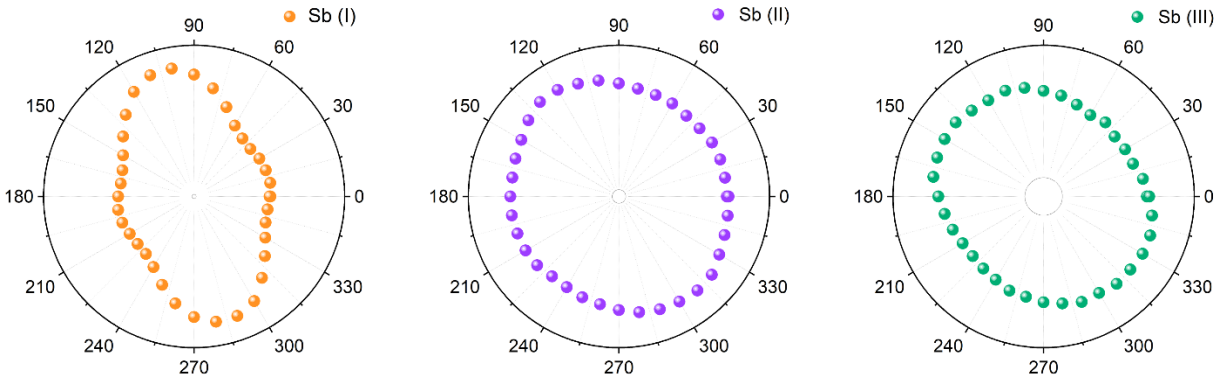

Figure S11 TPF intensities of the vertically placed crystals for various input polarization angles.

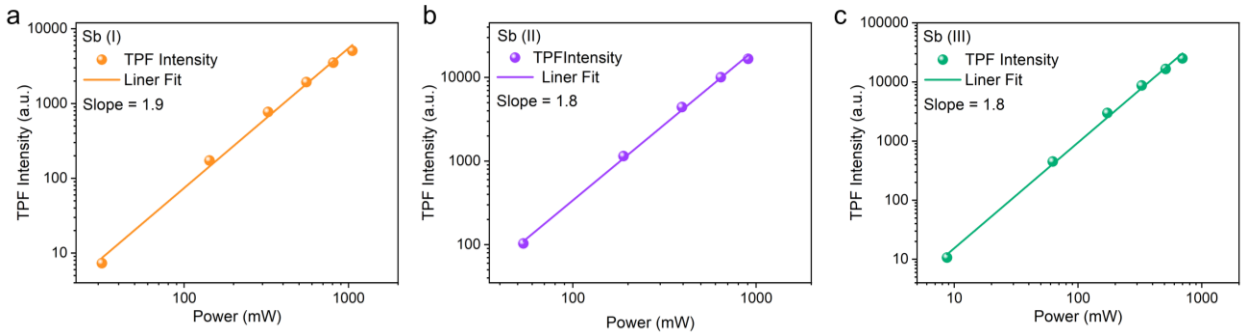

Figure S12 Logarithmic plots of TPF intensities as a function of the incident power, pumped at 800 nm. The solid line is a linear fit with a slope of ~2.0, confirming the two-photon characteristics of the TPF emission.

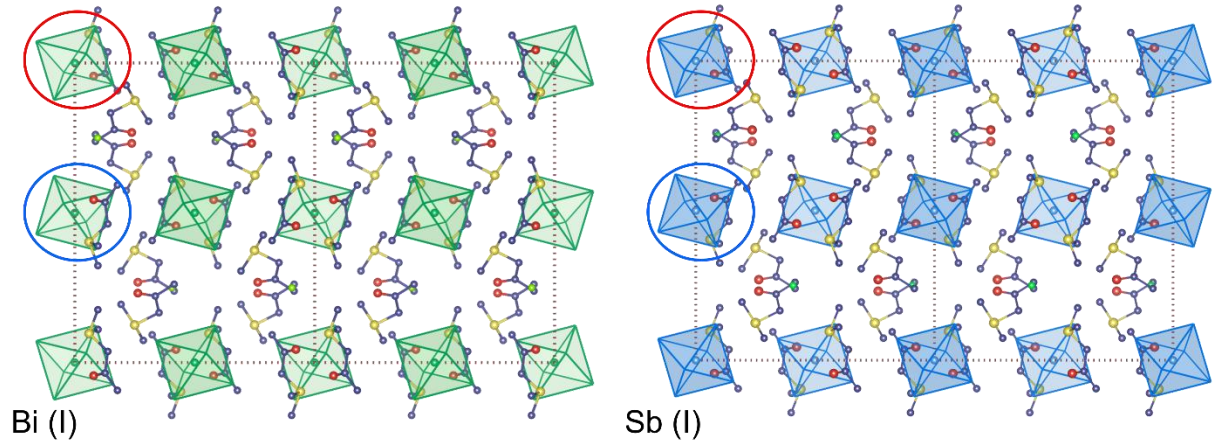

Figure S13 The two unit cells of Bi- and Sb-based OIHMH (I) reveal two dominant angular orientations of the $[SbBr_6]^{3-}$/$[BiBr_6]^{3-}$ octahedra within their respective lattices.

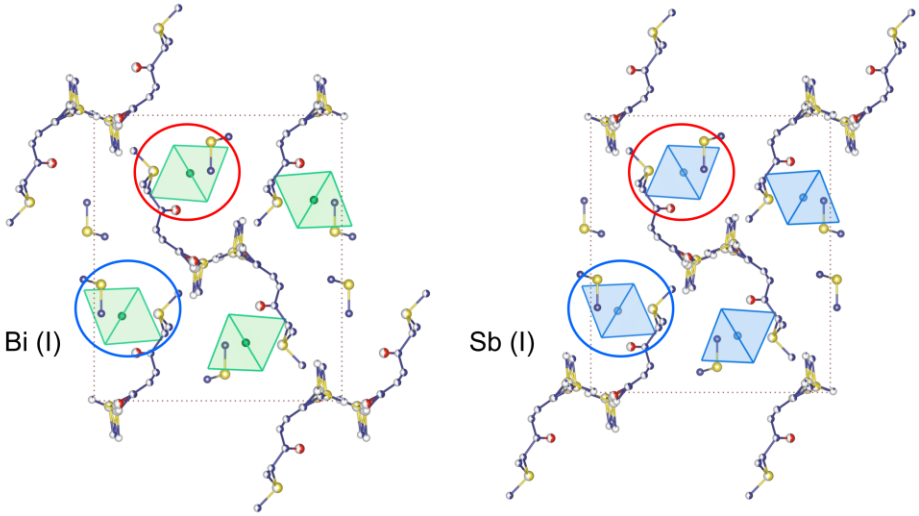

Figure S14 Unit cell of Bi- and Sb-based OIHMH (II) reveal two dominant angular orientations of the $[SbBr_6]^{3-}$/$[BiBr_6]^{3-}$ octahedra within their respective lattices.

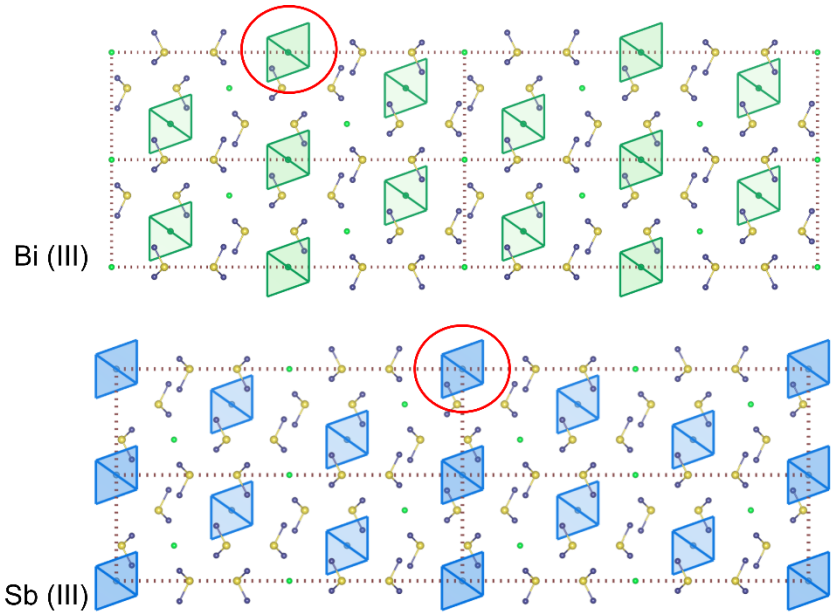

Figure S15 The four unit cells of Bi- and Sb-based OIHMH (III) reveal the unity dominant angular orientations of the $[SbBr_6]^{3-}$/$[BiBr_6]^{3-}$ octahedra within their respective lattices.

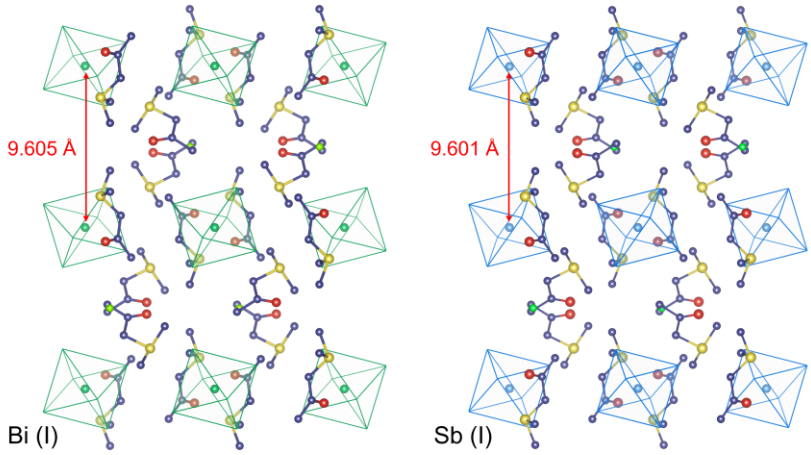

Figure S16 The Bi- and Sb-based OIHMH (I) compounds exhibit relatively large interlayer spacings of 9.605 Å and 9.601 Å, respectively.

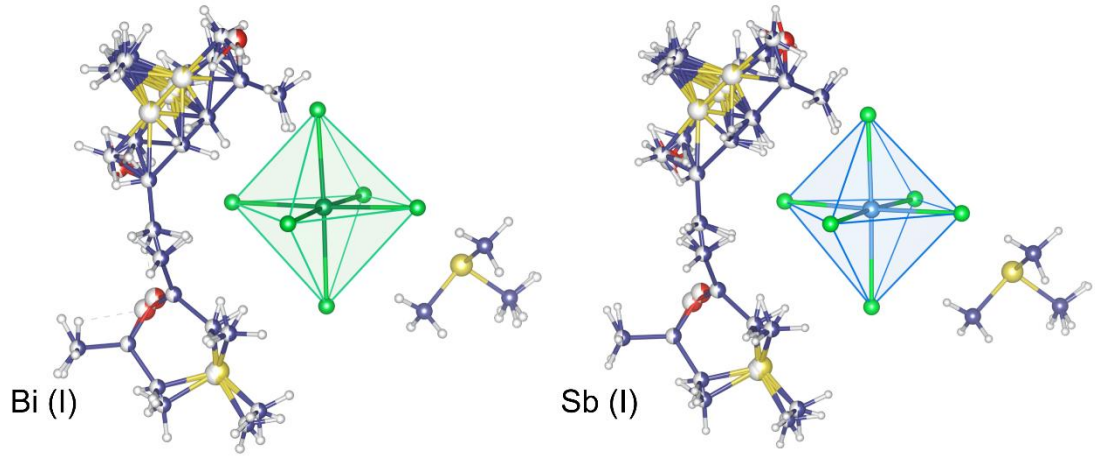

Figure S17 The minimum asymmetric units of Bi- and Sb-based OIHMH (II) show the incorporation of both the highly disordered $DOPS^+$ and TMS^+ cations in the lattice.

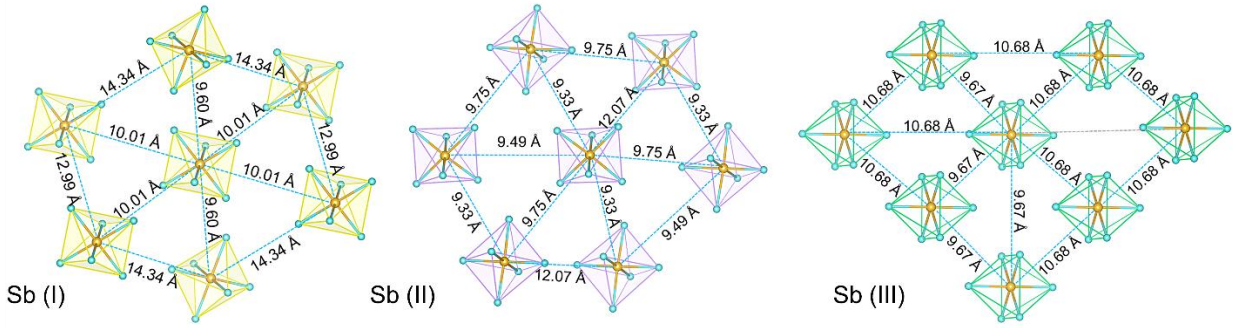

Figure S18 The metal-metal distances between adjacent inorganic components of Sb-based OIHMHs. Sb (II) exhibits a higher degree of freedom for rearrangement, while Sb (III) shows the most uniform distribution.

Supplementary Tables

Table S1.1 Crystal data and refinement results of the three Bi-based OIHMHs.

Identification	$(DOPS)_4[BiBr_6]Br$	$(DOPS)_2(TMS)[BiBr_6]$	$(TMS)_4[BiBr_6]Br$
CCDC	2514344	2514346	2514343
Empirical formula	$C_{20}H_{44}Br_7O_4S_4Bi$	$C_{13}H_{31}Br_6O_2S_3Bi$	$C_{12}H_{36}Br_7S_4Bi$
Formula weight	1245.14	1004.0	1076.99
Temperature (K)	100.01(11)	99.99(10)	99.98(11)
Crystal system	monoclinic	orthorhombic	trigonal
Space group	*C*2/*c*	*P*nma	*R*-3m
a (Å)	13.0429(4)	17.6226(3)	9.6747(4)
b (Å)	15.3355(4)	10.3599(2)	9.6747(4)
c (Å)	19.2095(5)	15.3149(3)	27.6343(10)
α (°)	90	90	90
β (°)	96.005(2)	90	90
γ (°)	90	90	120
V ($Å^3$)	3821.19(18)	2796.02(11)	2240.0(2)
Z	4	4	3
ρ (calculated) (g/cm^3)	2.164	2.367	2.395
F (000)	2352.0	1848.0	1500.0
R_{int}	0.0336	0.0408	0.0458
Goodness-of-fit on F^2	1.078	1.075	1.123
Final R indexes [I >= 2σ (I)]	$R_1 = 0.0218$ $wR_2 = 0.0531$	$R_1 = 0.0329$ $wR_2 = 0.0576$	$R_1 = 0.0241$ $wR_2 = 0.0587$

Table S1.2 Crystal data and refinement results of the three Sb-based OIHMHs.

Identification	$(DOPS)_4[SbBr_6]Br$	$(DOPS)_2(TMS)[SbBr_6]$	$(TMS)_4[SbBr_6]Br$
CCDC	2386943	2514345	2514342
Empirical formula	$C_{20}H_{44}Br_7O_4S_4Sb$	$C_{13}H_{31}Br_6O_2S_3Sb$	$C_{12}H_{36}Br_7S_4Sb$
Formula weight	1157.91	916.74	989.77
Temperature (K)	100.00	100.4(10)	99.98(10)
Crystal system	monoclinic	orthorhombic	trigonal
Space group	*C*2/*c*	*P*nma	*R*-3m
a (Å)	12.99290(10)	17.6067(3)	9.6670(6)
b (Å)	15.2323(2)	10.2896(2)	9.6670(6)
c (Å)	19.2027(2)	15.2631(3)	27.6665(13)
α (°)	90	90	90
β (°)	96.1550(10)	90	90
γ (°)	90	90	120
V ($Å^3$)	3778.53(7)	2765.15	2239.1(3)
Z	4	4	3
ρ (calculated) (g/cm^3)	2.035	2.176	2.202
F (000)	2224.0	1713.0	1404.0
R_{int}	0.0421	0.0274	0.0343
Goodness-of-fit on F^2	1.093	1.085	1.059
Final R indexes [I >= 2σ (I)]	$R_1 = 0.0310$ $wR_2 = 0.0872$	$R_1 = 0.0271$ $wR_2 = 0.0504$	$R_1 = 0.0324$ $wR_2 = 0.0623$

Table S2 Summary of the $[M]^+$ calculated for the dissolved three types of OIHMHs dissolved in H_2O.

Compound	$[M]^+$ calculated	Found
$(DOPS)_4[SbBr_6]Br$	119.0525 ($C5H11OS^+$)	119.0527
$(DOPS)_2(TMS)[SbBr_6]$	119.0525 ($C5H11OS^+$)	119.0525
	77.0419 ($C3H9S^+$)	77.0420
$(DOPS)_2(TMS)[BiBr_6]$	119.0525 ($C5H11OS^+$)	119.0525
	77.0419 ($C3H9OS^+$)	77.0420
$(TMS)_4[SbBr_6]Br$	77.0419 ($C3H9OS^+$)	77.0430

Table S3 Summary of E_g (experimentally determined value) for the resulting OIHMHs.

Compound	E_g	Compound	E_g
$(DOPS)_4[BiBr_6]Br$	3.00 eV	$(DOPS)_4[SbBr_6]Br$	3.03 eV
$(DOPS)_2(TMS)[BiBr_6]$	2.97 eV	$(DOPS)_2(TMS)[SbBr_6]$	3.01 eV
$(TMS)_4[BiBr_6]Br$	2.96 eV	$(TMS)_4[SbBr_6]Br$	2.98 eV

Table S4 Summary of decomposition temperature (T_d) for the resulting OIHMHs.

Compound	T_d	Compound	T_d
$(DOPS)_4[BiBr_6]Br$	142 °C	$(DOPS)_4[SbBr_6]Br$	110 °C
$(DOPS)_2(TMS)[BiBr_6]$	168 °C	$(DOPS)_2(TMS)[SbBr_6]$	164 °C
$(TMS)_4[BiBr_6]Br$	187 °C	$(TMS)_4[SbBr_6]Br$	207 °C

Table S5 Summary of PL, Stokes shift, FWHM, τ, PLQY for the three Sb-based OIHMHs.

Compound	PL (nm)	Stokes shift (nm)	FWHM (nm)	τ （μs）	PLQY
$(DOPS)_4[SbBr_6]Br$	563	190	120	1.47	100%
$(DOPS)_2(TMS)[SbBr_6]$	566	189	124	0.99	26.6%
$(TMS)_4[SbBr_6]Br$	560	187	119	0.97	41.2%

Table S6 Summary of Δl and σ^2 for the three types of OIHMHs.

Compound	Δl ($\times 10^{-4}$)	σ^2	Compound	Δl ($\times 10^{-4}$)	σ^2
$(DOPS)_4[BiBr_6]Br$	0.09	2.16	$(DOPS)_4[SbBr_6]Br$	0.12	1.84
$(DOPS)_2(TMS)[BiBr_6]$	0.89	3.73	$(DOPS)_2(TMS)[SbBr_6]$	2.39	3.59
$(TMS)_4[BiBr_6]Br$	0	0.03	$(TMS)_4[SbBr_6]Br$	0	0.04

Supplementary References

1. Tauc J, Menth A. States in the gap. *J Non-Cryst Solids* 1972; **8-10**: 569-585.
2. Xu J, Semin S, Niedzialek D *et al.* Self-assembled organic microfibers for nonlinear optics. *Adv Mater* 2013; **25**: 2084-2089.
3. Yuan C, Li X, Semin S *et al.* Chiral lead halide perovskite nanowires for second-order nonlinear optics. *Nano Lett* 2018; **18**: 5411-5417.